Electronic Supplementary Material (ESI) for Journal of Materials Chemistry B.

Support Information

Dual Amyloid Cross-Seeding Reveals Steric Zipper-Facilitated Fibrillization and Pathological Links between Protein Misfolding Diseases

Yanxian Zhang[1ζ], Mingzhen Zhang[1ζ], Yonglan Liu[1ζ], Dong Zhang[1], Yijing Tang[1], Baiping Ren[1], and Jie Zheng[1*]

[1]Department of Chemical, Biomolecular, and Corrosion Engineering
The University of Akron, Ohio, USA

ζ These authors contribute equally to this work.

* Corresponding author: zhengj@uakron.edu

Table S1. Summary of amyloid cross-seeding models between GNNQQNY-Aβ and between GNNQQNY-hIAPP in double-layer and triple-layer organizations. The classification of cross-seeding interface is defined by $[^{GY}O\text{-}C^{A\beta}]_{\uparrow\uparrow}$, $[^{GY}O\text{-}N^{A\beta}]_{\uparrow\downarrow}$, $[^{GY}E\text{-}C^{A\beta}]_{\uparrow\downarrow}$, $[^{GY}E\text{-}N^{A\beta}]_{\uparrow\downarrow}$ and $[^{GY}O\text{-}C^{hP}]_{\uparrow\uparrow}$, $[^{GY}O\text{-}N^{hP}]_{\uparrow\downarrow}$, $[^{GY}E\text{-}C^{hP}]_{\uparrow\downarrow}$, $[GY^{E\text{-}N}hP]_{\uparrow\downarrow}$, where the superscripted two letters represent amyloid peptide (GY=GNNQQNY, Aβ=Aβ, and hP=hIAPP); Capital letters of "O" and "E" represent the odd face containing G1, N3, Q5, Y7 residues and even face containing N2, Q4, N6 residues of GNNQQNY; Capital letters of "N" and "C" represent N-terminal and C-terminal β-sheet of Aβ or hIAPP; Symbols of "↑↑" and "↑↓" represent parallel and antiparallel orientations between GNNQQNY and Aβ/hIAPP.

System	Interface	dx (Å)	dy (Å)	Stability
A1	$[^{GY}\mathbf{O}\text{-}\mathbf{C}^{A\beta}]_{\uparrow\downarrow}$	-10.3	13.5	stable
A2	$[^{GY}\mathbf{E}\text{-}\mathbf{C}^{A\beta}]_{\uparrow\downarrow}$	-10.4	14.0	unstable
A3	$[^{GY}\mathbf{E}\text{-}\mathbf{C}^{A\beta}]_{\uparrow\downarrow}$	3.6	14.9	stable
A4	$[^{GY}\mathbf{E}\text{-}\mathbf{C}^{A\beta}]_{\uparrow\uparrow}$	-5.6	14.9	stable
A5	$[^{GY}\mathbf{O}\text{-}\mathbf{C}^{A\beta}]_{\uparrow\uparrow}$	-0.6	13.4	stable
A6	$[^{GY}\mathbf{O}\text{-}\mathbf{C}^{A\beta}]_{\uparrow\uparrow}$	9.5	13.5	unstable
A7	$[^{GY}\mathbf{E}\text{-}\mathbf{C}^{A\beta}]_{\uparrow\uparrow}$	11.3	14.9	unstable
A8	$[^{GY}\mathbf{O}\text{-}\mathbf{N}^{A\beta}]_{\uparrow\downarrow}$	-9.4	-14.5	unstable
A9	$[^{GY}\mathbf{E}\text{-}\mathbf{N}^{A\beta}]_{\uparrow\downarrow}$	-9.1	-14.9	unstable
A10	$[^{GY}\mathbf{O}\text{-}\mathbf{N}^{A\beta}]_{\uparrow\uparrow}$	11.1	-14.9	stable
A11	$[^{GY}\mathbf{E}\text{-}\mathbf{N}^{A\beta}]_{\uparrow\uparrow}$	13.0	-14.5	unstable
H1	$[^{GY}\mathbf{E}\text{-}\mathbf{C}^{hP}]_{\uparrow\downarrow}$	-14.8	-14.4	stable
H2	$[^{GY}\mathbf{O}\text{-}\mathbf{C}^{hP}]_{\uparrow\downarrow}$	-13.9	-14.1	stable
H3	$[^{GY}\mathbf{O}\text{-}\mathbf{C}^{hP}]_{\uparrow\downarrow}$	-4.9	-15.0	stable
H4	$[^{GY}\mathbf{E}\text{-}\mathbf{C}^{hP}]_{\uparrow\downarrow}$	-3.9	-16.2	stable
H5	$[^{GY}\mathbf{O}\text{-}\mathbf{C}^{hP}]_{\uparrow\downarrow}$	9.3	-13.9	unstable
H6	$[^{GY}\mathbf{E}\text{-}\mathbf{C}^{hP}]_{\uparrow\downarrow}$	12.1	-14.2	unstable
H7	$[^{GY}\mathbf{E}\text{-}\mathbf{C}^{hP}]_{\uparrow\uparrow}$	-21.3	-16.2	stable
H8	$[^{GY}\mathbf{E}\text{-}\mathbf{C}^{hP}]_{\uparrow\uparrow}$	-9.3	-15.3	stable
H9	$[^{GY}\mathbf{O}\text{-}\mathbf{C}^{hP}]_{\uparrow\uparrow}$	-7.2	-15.0	stable
H10	$[^{GY}\mathbf{O}\text{-}\mathbf{C}^{hP}]_{\uparrow\uparrow}$	2.8	-15.0	unstable
H11	$[^{GY}\mathbf{E}\text{-}\mathbf{N}^{hP}]_{\uparrow\downarrow}$	-4.1	13.1	unstable
H12	$[^{GY}\mathbf{O}\text{-}\mathbf{N}^{hP}]_{\uparrow\downarrow}$	-3.3	11.9	unstable
H13	$[^{GY}\mathbf{E}\text{-}\mathbf{N}^{hP}]_{\uparrow\downarrow}$	9.8	13.2	stable
H14	$[^{GY}\mathbf{E}\text{-}\mathbf{N}^{hP}]_{\uparrow\uparrow}$	5.1	13.2	unstable
AGA1	$[^{A\beta}\mathbf{C}\text{-}\mathbf{O}^{GY}\mathbf{E}\text{-}\mathbf{N}^{A\beta}]$	-	-	stable
AGA2	$[^{A\beta}\mathbf{C}\text{-}\mathbf{O}^{GY}\mathbf{E}\text{-}\mathbf{C}^{A\beta}]$			unstable
HGH1	$[^{hP}\mathbf{N}\text{-}\mathbf{E}^{GY}\mathbf{O}\text{-}\mathbf{C}^{hP}]$	-	-	stable
HGH2	$[^{hP}\mathbf{C}\text{-}\mathbf{E}^{GY}\mathbf{O}\text{-}\mathbf{C}^{hP}]$			unstable

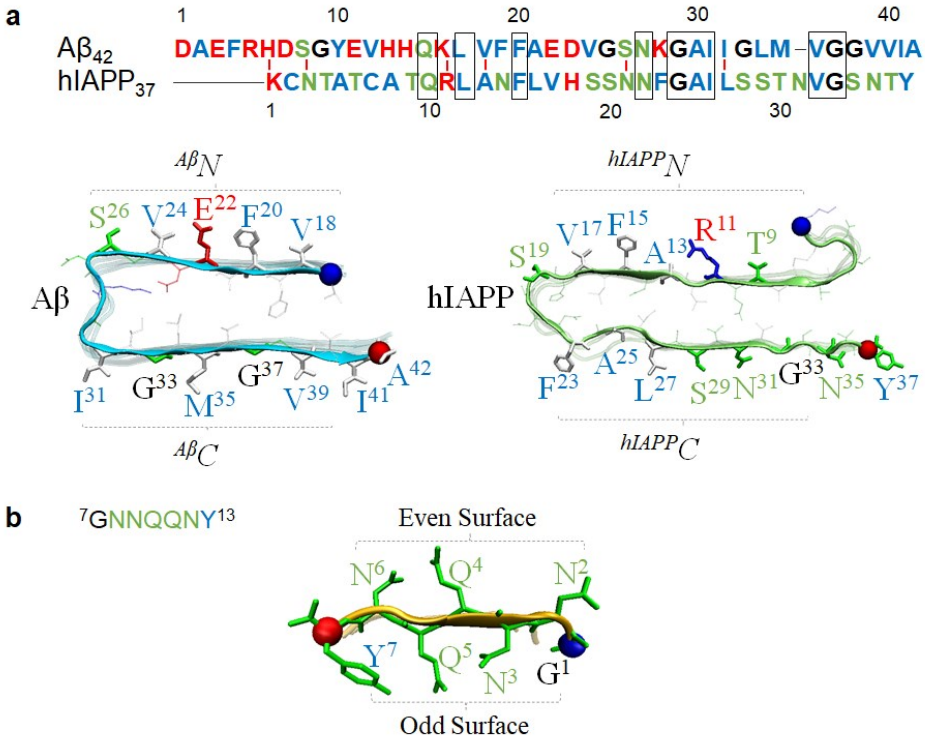

Figure S1. (**a**) Sequence and structural comparison between Aβ and hIAPP. Short red lines and black boxes indicate similar and same sequences between Aβ and hIAPP, respectively. (**b**) Sequence and structure of GNNQQNY. Three crystal fibrillar structures of Aβ, hIAPP, and GNNQQNY exhibit typical β-sheet structures, which provide a possible structural motif for amyloid cross-seeding between them. Color ID: charged residues in red, polar residues in green, and hydrophobic residues in blue.

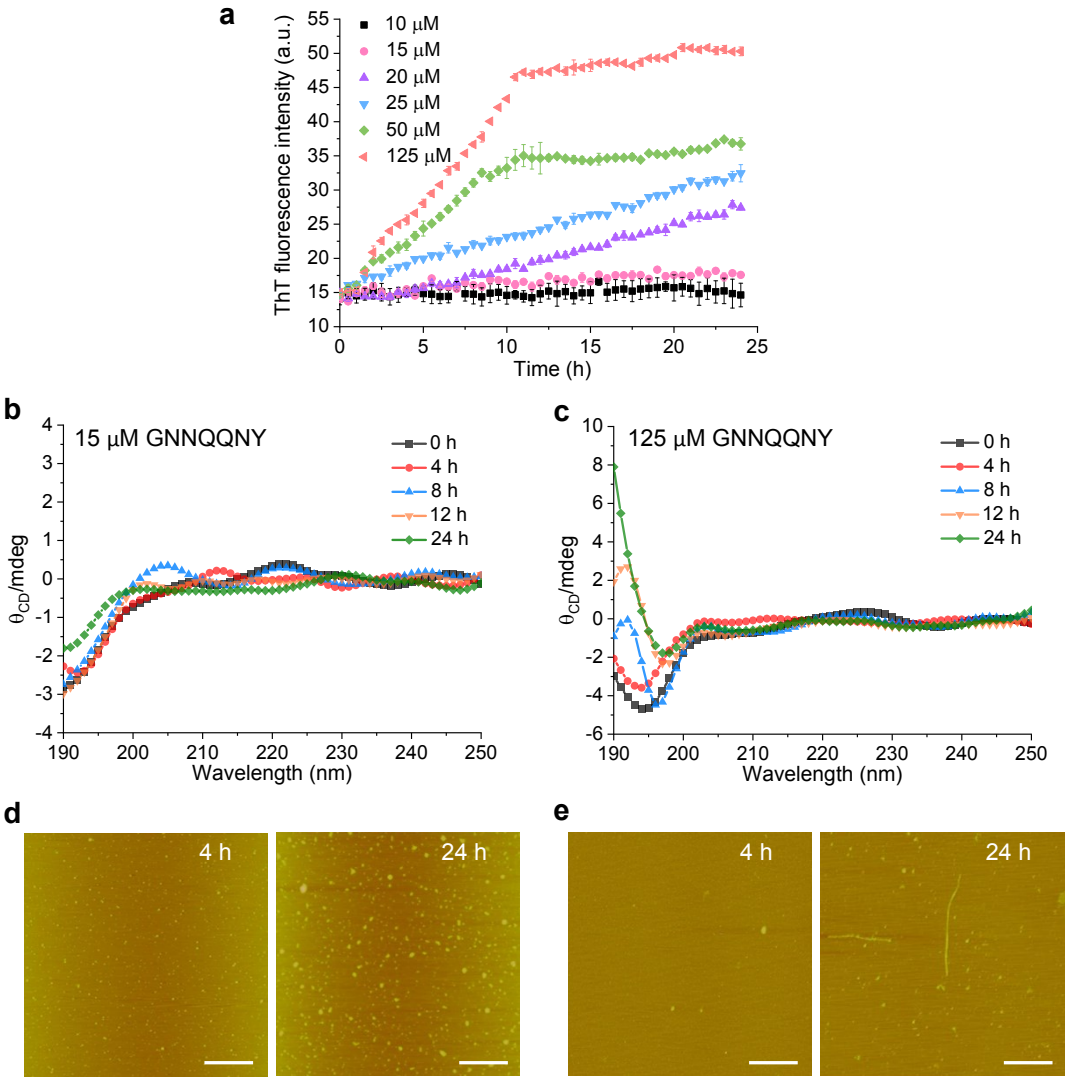

Figure S2. Concentration-dependent amyloidogenic property of GNNQQNY. (**a**) Time-dependent ThT fluorescence curves to monitor the aggregation kinetics of pure GNNQQNY at different concentrations of 10-125 μM. Self-aggregation of (**b, d**) 15 μM and (**c, e**) 125 μM GNNQQNY as monitored by (**b, c**) time-dependent far-UV CD spectra and (**d, e**) AFM images at 4 and 24 h.

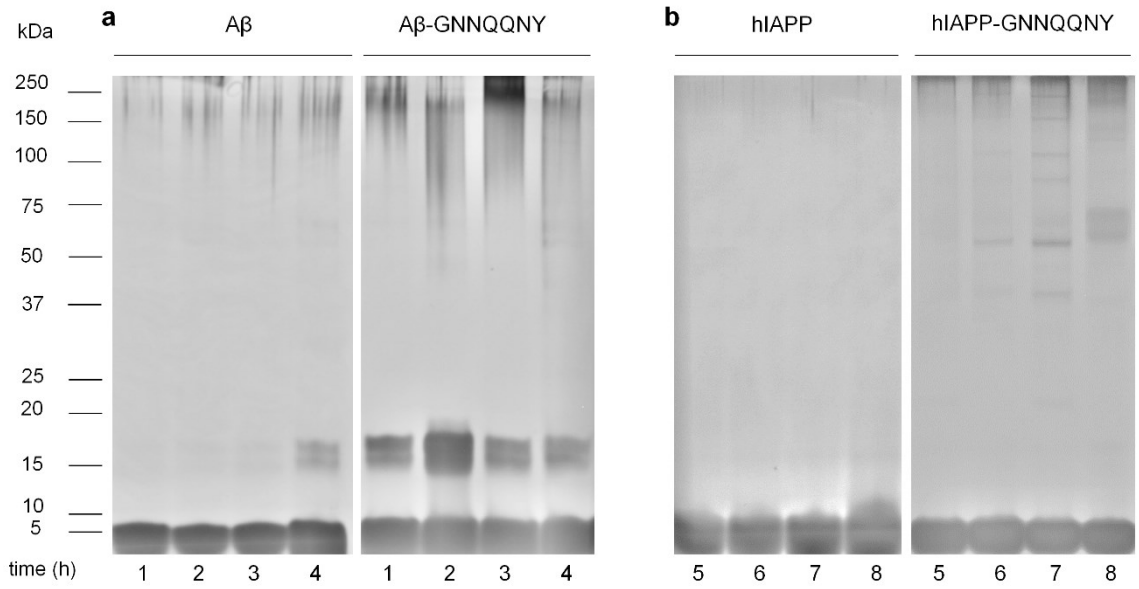

Figure S3. Characterization of pure and cross-seeding amyloid aggregates by SDS-PAGE. SDS-PAGE bands of (**a**) pure Aβ (15 μM) and cross-seeding Aβ-GNNQQNY (15 μM:15 μM) aggregates within 1-4 h and (**b**) pure hIAPP (15 μM) and cross-seeding hIAPP-GNNQQNY (15 μM:15 μM) aggregates within 5-8 h.

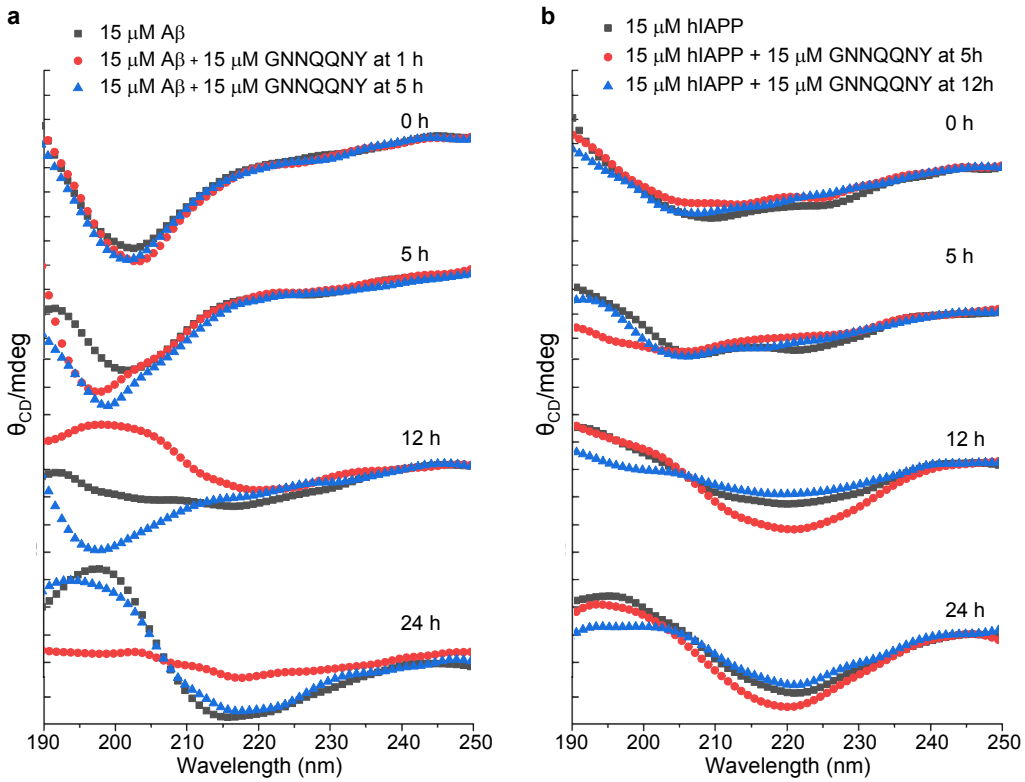

Figure S4. Time-dependent circular dichroism spectra for monitoring the secondary structure changes by adding GNNQQNY (15 μM) to (**a**) Aβ (15 μM) and (**b**) hIAPP (15 μM) seeds at different time points.

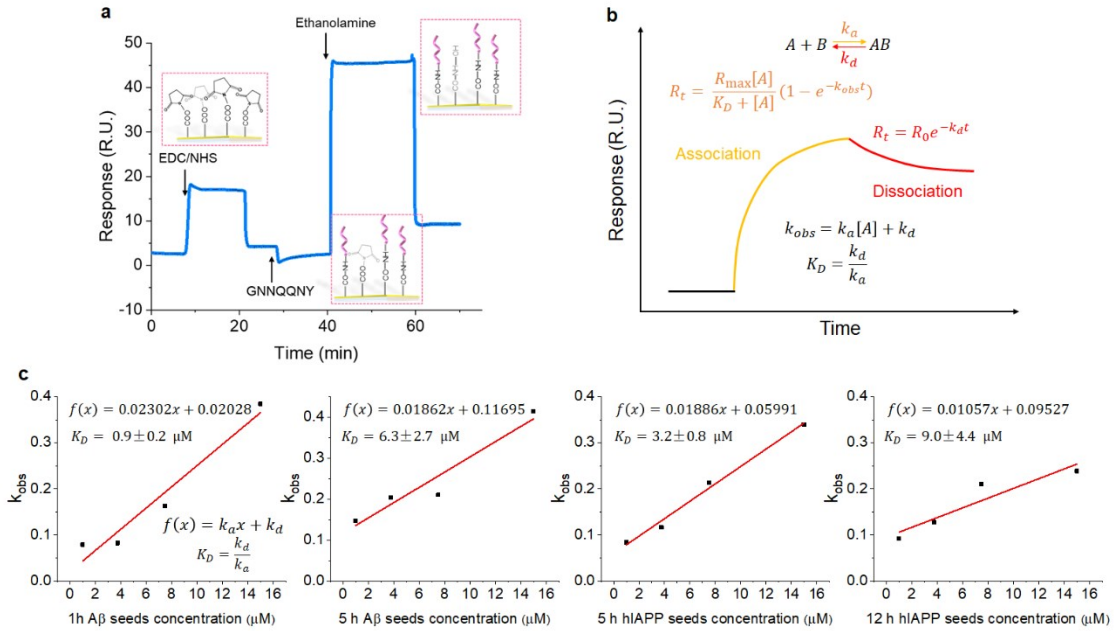

Figure S5. SPR sensorgram for monitoring binding affinity of GNNQQNY to Aβ or hIAPP seeds. (**a**) Representative SPR sensorgram to demonstrate the immobilization of GNNQQNY onto a gold chip via the EDC/NHS coupling method. (**b**) Schematic illustration to show the association and dissociation sensorgram phases and to determine association constant (k_a), dissociation constant (k_d), and binding constant ($K_D = k_d/k_a$) based on the Langmuir model. (**c**) Fitting the binding curves at different Aβ/hIAPP concentrations.

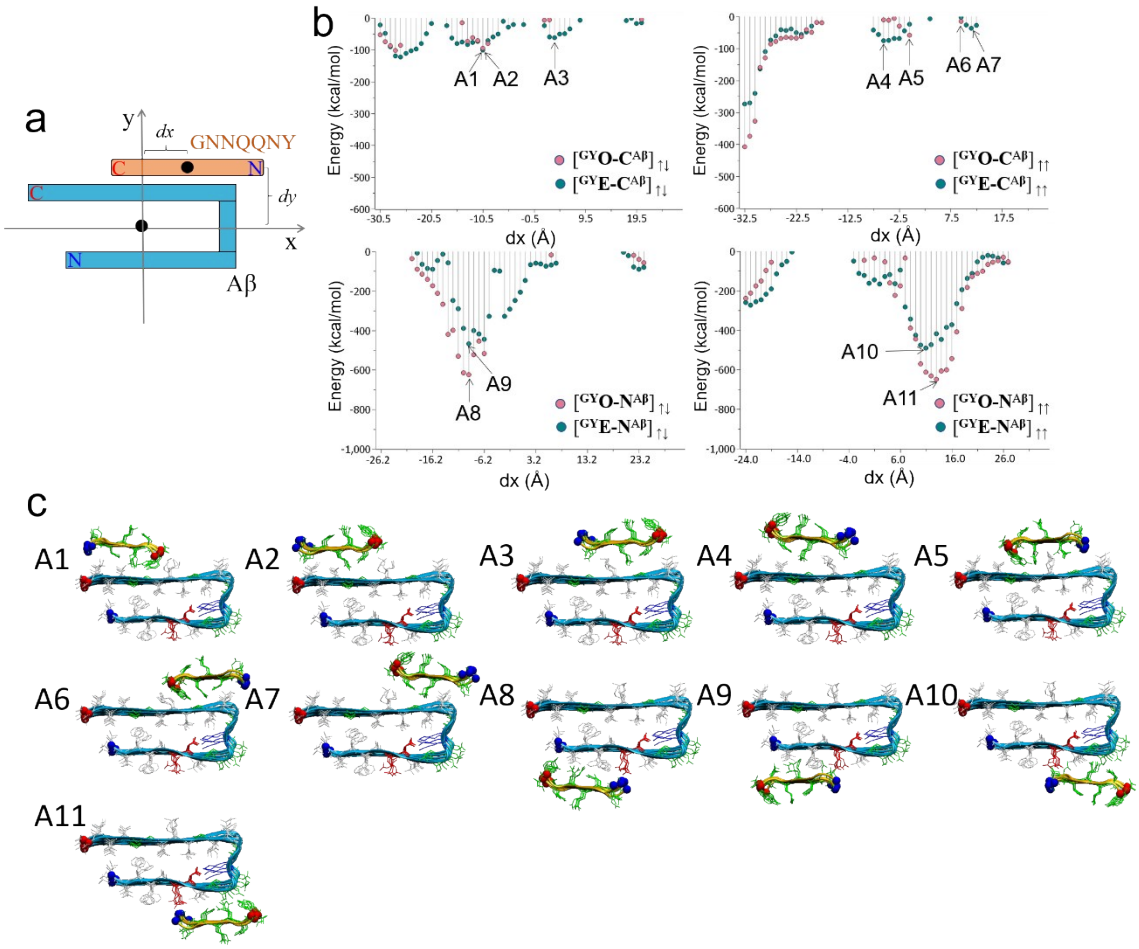

Figure S6. Interfacial scanning to determine the double-layer GNNQQNY-Aβ cross-seeding assemblies at the low energy states using an in-house peptide-packing program. (a) Interfacial scanning procedure for searching all possible cross-seeding interfaces between GNNQQNY and Aβ. (b) Packing energy profiles of all possible GNNQQNY-Aβ interfaces by considering four key parameters of interlayer translation (d_x), interlayer distance (d_y), layer-to-layer orientation (parallel vs. antiparallel), and interfacial sidechain contacts (even face vs. odd face of GNNQQNY). (c) Molecular structures of eleven double-layer GNNQQNY-Aβ assemblies at the low energy states, as selected from b.

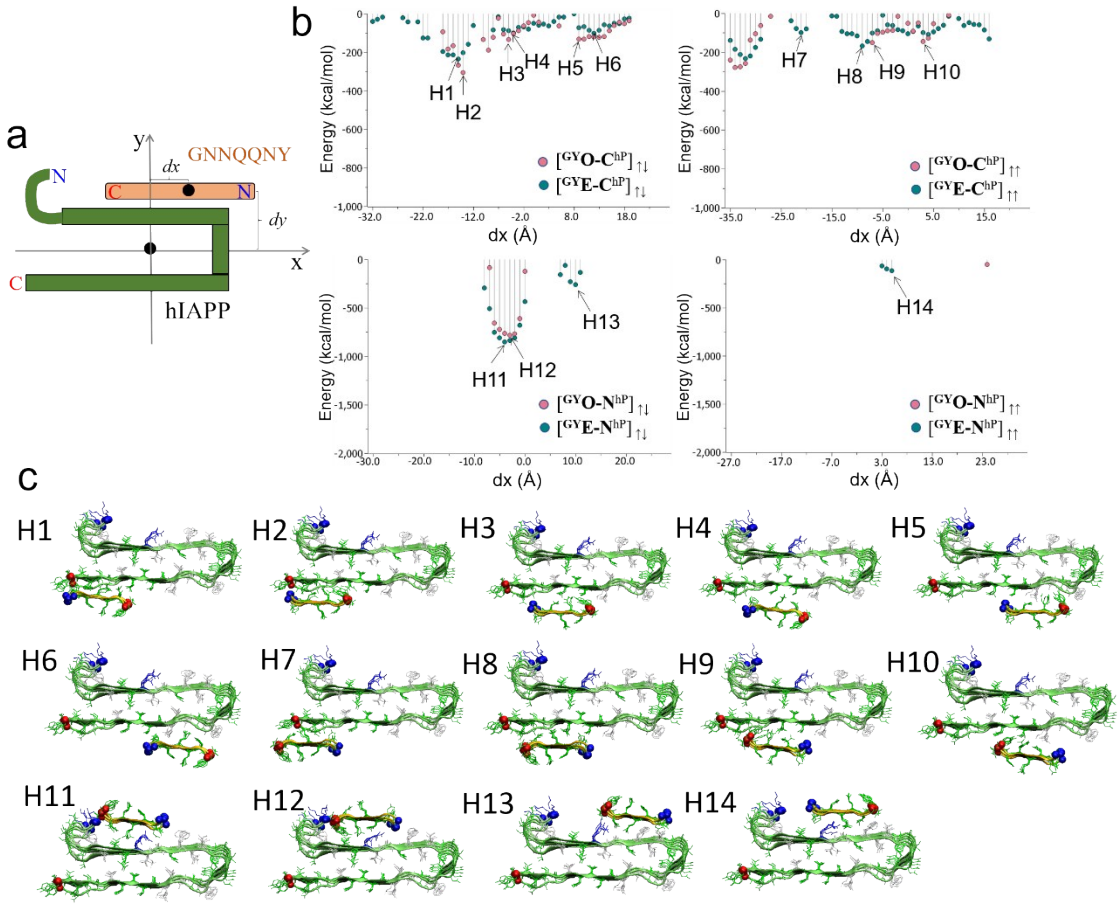

Figure S7. Interfacial scanning to determine the double-layer GNNQQNY-hIAPP cross-seeding assemblies at the low energy states using an in-house peptide-packing program. (**a**) Interfacial scanning procedure for searching all possible cross-seeding interfaces between GNNQQNY and hIAPP. (**b**) Packing energy profiles of all possible GNNQQNY-hIAPP interfaces by considering four key parameters of interlayer translation (d_x), interlayer distance (d_y), layer-to-layer orientation (parallel vs. antiparallel), and interfacial sidechain contacts (even face vs. odd face of GNNQQNY). (**c**) Molecular structures of fourteen double-layer GNNQQNY-hIAPP assemblies at the low energy states, as selected from **b**.

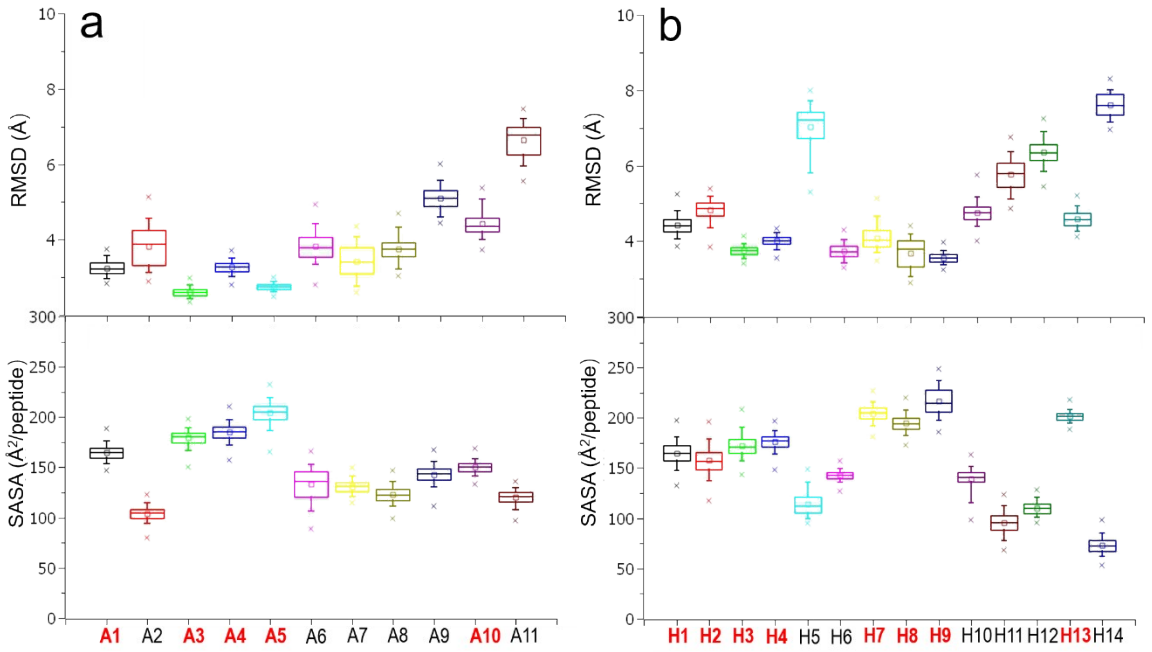

Figure S8. Structural and interfacial characterization of double-layer cross-seeding assemblies. RMSD and SASA values for (**a**) GNNQQNY-Aβ and (**b**) GNNQQNY-hIAPP assemblies as calculated from the last 25 ns trajectories. The systems with the lower RMSD and the higher SASA are initially selected as the most possible double-layer assemblies, leading to A1, A3, A4, A5 and A10 for GNNQQNY-Aβ and H1, H2, H3, H4, H7, H8, H9 and H13 for GNNQQNY-hIAPP.

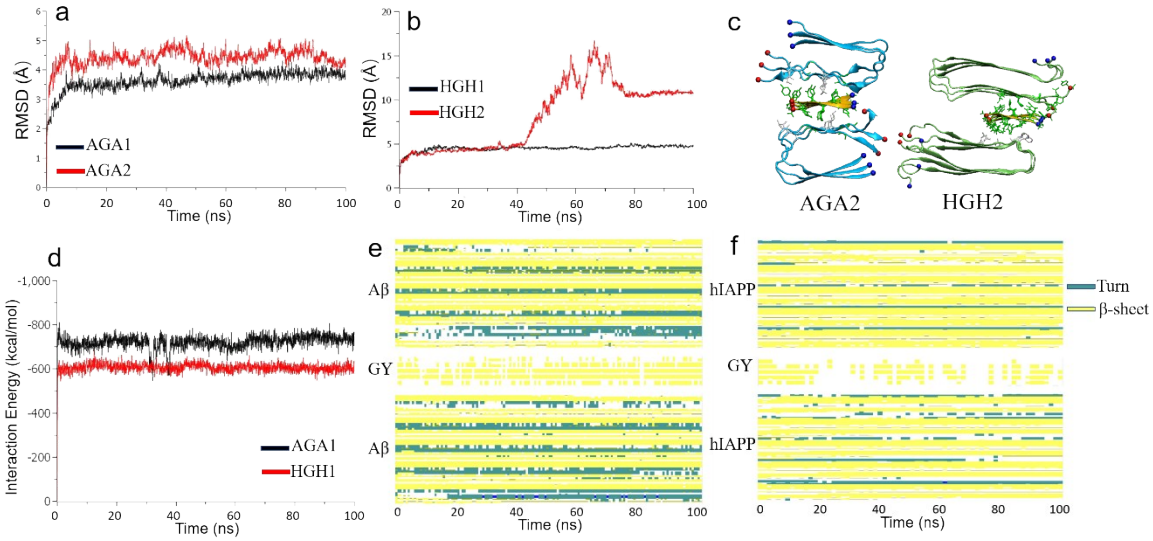

Figure S9. Structural and interfacial characterization of triple-layer cross-seeding assemblies. Time-dependent RMSD curves for (**a**) Aβ-GNNQQNY-Aβ (AGA1, AGA2), (**b**) hIAPP-GNNQQNY-hIAPP (HGH1, HGH2). (**c**) Representative MD snapshots of AGA2 and HGH2 assemblies, which are less stable than AGA1 and HGH1 assemblies. (**d**) Nonbonded interaction energies and (**e-f**) the secondary structures of AGA1 and HGH1 assemblies reveal strong interfacial interactions and highly stable secondary structures.

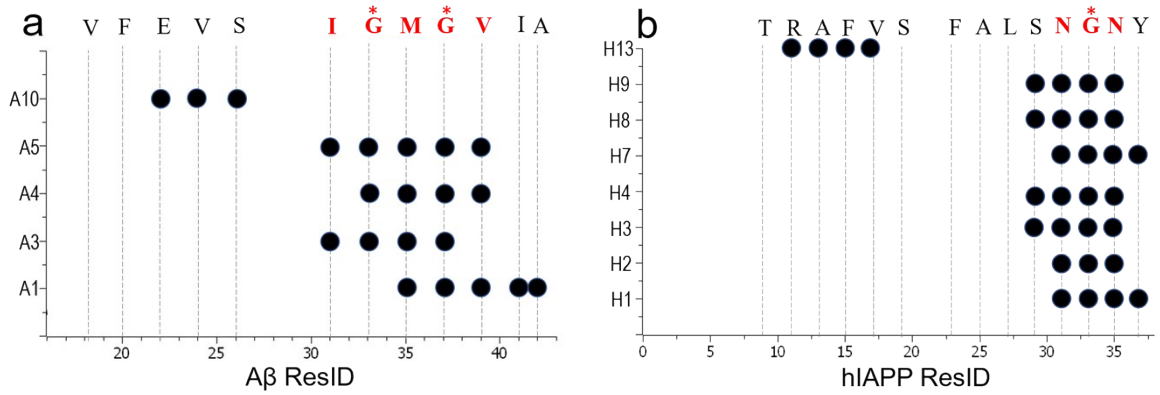

Figure S10. Interfacial residue contacts between double-layer (**a**) GNNQQNY-Aβ and (**b**) GNNQQNY-hIAPP assemblies.

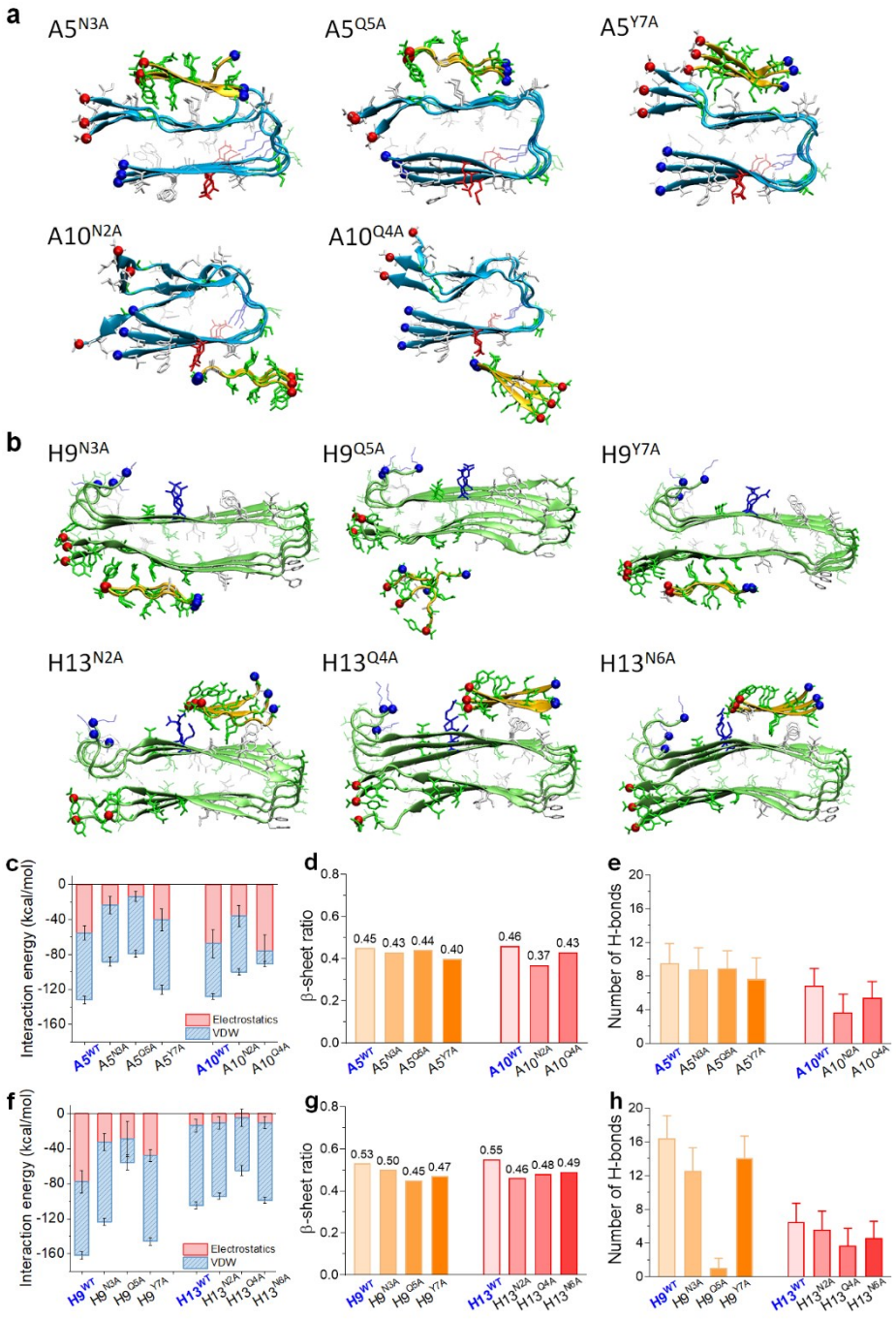

Figure S11. Structural and interfacial characterization of cross-seeding of GNNQQNY mutants with Aβ or hIAPP. Final molecular structures of cross-seeding of different GNNQQNY mutants with (**a**) Aβ in A5 and A10 models and (**b**) hIAPP in H9 and H13 models. Comparison of (**c, f**) nonbonded interaction energy, (**d, g**) β-sheet ratio, (**e, h**) number of hydrogen bonds between (**c, d, e**) wild type and mutants of GNNQQNY-Aβ assemblies and (**f, g, h**) wild type and mutants of GNNQQNY-hIAPP assemblies. All values in (**c-h**) are obtained and averaged from the last 20-ns MD simulations.

References